

Distribution Agreement

In presenting this thesis as a partial fulfillment of the requirements for a degree from Emory University, I hereby grant to Emory University and its agents the non-exclusive license to archive, make accessible, and display my thesis in whole or in part in all forms of media, now or hereafter now, including display on the World Wide Web. I understand that I may select some access restrictions as part of the online submission of this thesis. I retain all ownership rights to the copyright of the thesis. I also retain the right to use in future works (such as articles or books) all or part of this thesis.

Ruohe Wang

April 10, 2023

Theoretical Simulation of K-Edge X-Ray Absorption Spectra for Methane and Its Fluorinated
Derivatives

by

Ruohe Wang

Francesco A. Evangelista
Adviser

Chemistry

Francesco A. Evangelista
Adviser

Katherine M. Davis
Committee Member

Michael Heaven
Committee Member

2023

Theoretical Simulation of K-Edge X-Ray Absorption Spectra for Methane and Its Fluorinated
Derivatives

By

Ruohe Wang

Francesco A. Evangelista

Adviser

An abstract of
a thesis submitted to the Faculty of Emory College of Arts and Sciences
of Emory University in partial fulfillment
of the requirements of the degree of
Bachelor of Science with Honors

Chemistry

2023

Abstract

Theoretical Simulation of K-Edge X-Ray Absorption Spectra for Methane and Its Fluorinated Derivatives

By Ruohe Wang

X-ray absorption spectroscopy (XAS) has been widely studied as an element-specific technique to determine the electronic properties of molecules. Experiments have been conducted on methane and its fluorinated derivatives, a family of chemicals with significant impact in chemistry and environmental science, to investigate their electronic properties. With the development of advanced computational techniques, the electronic nature of the core excitations involved in XAS can be better understood. In this experiment, we employ both the time-dependent density functional theory (TDDFT), a single-reference density-based method, and the multiconfigurational self-consistent field (MCSCF) with the generalized active space self-consistent field method (GASSCF) as a reference to simulate the carbon and fluorine K-edge X-ray near edge spectra (XANES) of $\text{CH}_n\text{F}_{4-n}$ ($n=0-4$). We compare the two methods with experimental data to investigate the excitation contribution to the spectral features. We also analyze the spectra to explore how electronic properties can be reflected in the spectra.

Theoretical Simulation of K-Edge X-Ray Absorption Spectra for Methane and Its Fluorinated
Derivatives

By

Ruohe Wang

Francesco A. Evangelista

Adviser

A thesis submitted to the Faculty of Emory College of Arts and Sciences
of Emory University in partial fulfillment
of the requirements of the degree of
Bachelor of Science with Honors

Chemistry

2023

Acknowledgements

I would like to thank Dr. Evangelista for letting me work during the summer in his lab to learn about modern quantum chemistry methods, which introduced me to computational chemistry that combines my interest in chemistry and computer science. I am also grateful that he gave me the opportunity to conduct this research. In addition, I want to thank Kevin Marin, my graduate student mentor in the group, for guiding me patiently throughout the research when I was lost in the project. I would also like to thank all the lab members in the group that helped me when I was in doubt and taught me patiently given my limited knowledge.

Table of Contents

1. Introduction	
1.1 X-ray Spectroscopy Theory	1
1.2 Methane and Its Fluorinated Derivatives	
1.2.1 Overview	2
1.2.2 Environmental Impacts	3
1.3 Purpose	4
2. Computational Methods	
2.1 Geometry Optimization and Energy Determination	5
2.2 Time-dependent Density Functional Theory	
2.2.1 Background	6
2.2.2 Computation Setup	7
2.3 Multiconfigurational Self-Consistent Field Method	
2.3.1 Background	7
2.3.2 Computation Setup	9
3. Results	
3.1 Geometry and Energetics	10
3.2 XANES Spectral Features	10
3.3 Excitation Contribution	11
4. Discussion	12
5. Code Availability	13
6. Reference	14
7. Tables/Figures/Schemes	17

1. Introduction

1.1 X-ray Spectroscopy Theory

X-ray spectroscopy has been investigated extensively to understand the system of interest. X-ray radiation provides photons with energy from around 100 eV to 1000 keV and can excite electrons in a molecule to a state with higher energy. One of the most critical types of X-ray spectroscopy is X-ray absorption spectroscopy (XAS), which measures the energy absorbed during the electronic transition from the core orbitals to unoccupied orbitals (i.e. bound states) or the continuum (i.e. unbound states).¹ The spectral region related to the former one is named X-ray absorption near-edge structure (XANES) and extended X-ray absorption fine structure (EXAFS) for the latter. A near-edge region can be further divided into a pre-edge region due to the excitations from *s* to the partially unfilled *d*-orbitals for the transition metals and a rising edge slightly above the binding energy of the core electron. Depending on the electron shell from which the core electron is excited, the spectra can be categorized into K-edge, L-edge, and M-edge spectra for $n = 1, 2,$ and $3,$ etc.

The selection rule of X-ray absorption is $\Delta L = \pm 1, 0, \Delta J = \pm 1, 0,$ and $\Delta S = 0$ based on the dipole moment.² In addition, the electronic transitions with $\Delta L = \pm 2$ (e.g., $1s \rightarrow 3d$) are quadrupole-allowed with a noticeable intensity for the transition metals with incomplete *d*-orbitals due to their large electron density. Based on the selection rule, the excitations from the $1s$ or $2s$ orbitals can probe the *p*-character of the transition, while those from the $2p$ orbitals can determine the *d*- and *s*-character of a transition. The intensity of the absorption peak for a transition from the initial state $|\psi_i\rangle$ to the final state $|\psi_f\rangle$ is positively correlated with the dipole

moment according to the Golden Fermi Rule, where the $\hat{e} \cdot r$ is the dipole moment operator and ρ is the density of the continuum state.

$$I \propto |\langle \psi_f | \hat{e} \cdot r | \psi_i \rangle|^2 \rho(E) \quad (1)$$

Due to the ability to probe the core-excited electronic states, much useful information can be obtained regarding the molecule's electronic properties, including oxidation states, bond lengths, and coordination symmetry.

1.2 Methane and Its Fluorinated Derivatives

1.2.1 Overview

Methane and its fluorinated derivatives ($\text{CH}_n\text{F}_{4-n}$, $n = 0-4$) are involved in various contexts in chemistry. As the simplest organic compound, methane has been extensively studied, including various essential chemical reactions.³ Research has also been conducted on the fluorinated derivatives of methane. For instance, they have been utilized to investigate the fluorination of organic compounds in a laboratory setting, with the development of many effective reactions introducing extra fluorine groups.⁴

This family of molecules is often employed as a model system in computational chemistry due to the progressively increasing electronic complexity introduced by the increasing number of fluorine atoms. With the emergence of powerful computational techniques, their physical and chemical properties have been determined, such as the equilibrium geometry, bond order, and incremental geminal stabilization.^{5,6} It was found that the gradual substitution of fluorine atoms can change the dipole moment of the molecule and lead to a progressive shrinkage of the C-F bond length, advancing the understanding of its reactivity.

1.2.2 *Environmental Impacts*

Much attention has been paid to the environmental impacts of the fluorinated derivatives of methane. These compounds are widely employed as refrigerants and represent the class of chemicals known as hydrofluorocarbons (HFCs). The evolution of refrigerants is directed toward the minimization of environmental influences, particularly ozone depletion and global warming. Chlorofluorocarbons (CFCs) were first synthesized to replace the earlier refrigerants with lowered combustibility and toxicity.⁷ These refrigerants, however, can lead to the depletion of the stratospheric ozone layer that protects terrestrial life from the high-energy UV radiation reaching the Earth's surface. Chlorine atoms can be released with the presence of high-energy photons and convert ozone molecules readily to oxygen.

Chemicals like hydrochlorofluorocarbons (HCFCs) were developed to reduce the ozone depletion potential. Alternative refrigerants, including HFCs, were then proposed as third-generation refrigerants with almost no negative effects on the ozone layer. Nonetheless, the global warming issue resulting from the use of these compounds persists. These molecules can absorb infrared radiation from the ground to space, allowing the heat to accumulate with an increased temperature of the surface and atmosphere of the Earth. These fluorinated gases (F-gases) are thus under the regulation of many global environmental policies such as the Kyoto Protocol, the Montreal Protocol, and the regulations of the European Union (EU).⁸ Although the fourth-generation refrigerants with low global warming potential are in active development to phase out the previous ones, HFCs still contribute to a large proportion of emissions in many countries.^{9,10}

1.3 Purpose

Experiments related to X-ray spectroscopy have been continuously conducted with the development of instruments to produce the X-ray radiation source. For instance, the development of the synchrotron, an instrument that can accelerate the photon to almost the speed of light, allows the study of many interesting molecules, including methane and its fluorinated derivatives.¹¹⁻¹⁵ These investigations allow a further understanding of their electronic properties from an experimental perspective and serve as an essential reference for theoretical studies. In the experimental XAS studies, the peaks are often assigned to an electronic transition from the core orbital to a single unoccupied orbital with high interpretability. Similarly, many computational methods use the single reference method, which only considers the excitations from the ground state with a single configuration, including the Hartree-Fock (HF) self-consistent field method and time-dependent density functional theory (TDDFT).

With the rising of state-of-the-art multireference methods, such as the multiconfigurational self-consistent field (MCSCF) theory, it becomes possible to utilize more advanced methods with higher accuracy and better predictive power to describe molecular systems. These methods take into account the nondynamic correlations among the electrons described by a wave function in the form of a linear combination of multiple Slater determinants constructed from the ground state with comparable coefficients. They are thus known to be capable of describing the excited states better compared to the single-reference methods.^{16,17}

With the newly developed computational techniques, only a few studies have simulated the XANES spectra to compare with the experimental XANES data and analyzed the core-excited electronic states. In this study, we focus on the excitations from both the carbon 1s and

fluorine 1s orbitals to the bound states in the $\text{CH}_n\text{F}_{4-n}$ system and simulate the K-edge X-ray absorption spectrum for each molecule using both the single-reference TDDFT method and the multireference driven similarity renormalization group at the third-order perturbation theory level (DSRG-MRPT3) method with a reference known as generalized active space self-consistent field (GASSCF) method. The performance of the two methods on this system can thus be compared in terms of accuracy and complexity. The contribution of each excited electronic state to the main peaks can be analyzed to assign the peaks and discover any potential trend for the molecules with progressively introduced fluorine atoms. It is also of interest to determine whether the electronic properties of the molecules can be reflected on XANES and vice versa, enhancing the ability to interpret X-ray absorption spectra.

2. Computational Methods

The calculations in this study were performed using the packages Psi4¹⁸, ORCA¹⁹, and Forte²⁰ with Avogadro²¹ as the visualization tool.

2.1 Geometry Optimization and Energy Determination

The geometry of the molecules was optimized at the coupled-cluster singles, doubles, and perturbative triples level of theory [CCSD(T)] with the cc-pCVDZ^{22,23} basis set to find the stationary point with the lowest total energy using Psi4. Frequency analysis was performed at the same theoretical level to characterize the stationary points and determine the zero-point vibrational energy (ZPVE) correction. Avogadro was utilized to visualize the equilibrium geometries and determine the C-H and C-F bond lengths. The orbital energy for each molecule was calculated using the Hartree-Fock (HF) self-consistent field with the cc-pCVQZ-DK basis set and visualized as molecular diagrams for analysis.

2.2 Time-dependent Density Functional Theory

2.2.1 Background

Time-dependent density functional theory is based on the density functional theory (DFT) with the addition of time dependence. DFT considers the total energy of a system as a function of the electron density.^{24,25} Under the Kohn-Sham approximation, the electrons only interact with the complete electron density of the system rather than individually, so the energy can further be categorized into non-interacting energy (kinetic energy), potential energy due to classical electrostatic interactions ($V_{ee} + V_{eN}$), and interaction energy as shown in the equation below.

$$E[\rho] = T[\rho] + V_{ee}[\rho] + V_{eN}[\rho] + E_{xc}[\rho] \quad (2)$$

The third term in Equation (2) is often generalized as an external potential and can be expressed as $\int \rho(r) V_{ext}(r) dr$. The last term is known as the exchange-correlation functional, a correction to account for the energy neglected in the approximation. Since the electrons are assumed to be independent, a Kohn-Sham operator can be defined for each electron. The energy of the whole system can then be expressed as a sum of energy for each electric density.

DFT cannot effectively describe the excited states due to the lack of a one-to-one correspondence between the density and the potential, so improvements have been made to DFT for the excitation problem, including TDDFT. With the time dependence, the energy can then be calculated using the formula below, where \hat{V} represents the one-particle electron potential.¹⁶

$$E = \sum_i^N [\langle \psi_i | \hat{T} + \hat{V}(r, t) | \psi_i \rangle + A_{xc}[\rho(r, t)]] \quad (3)$$

2.2.2 Computation Setup

The electric dipole, magnetic dipole, and electric quadruples for each core-excited electronic state were determined on the optimized geometries using the time-dependent density functional theory (TDDFT) method with the B3LYP functional^{26,27} and the cc-pVQZ-DK basis set^{22,28} under the Tamm-Dancoff approximation (TDA) using ORCA. The electron was allowed to be excited from the core orbital of interest (C 1s or F 1s) to any unoccupied orbital. The calculated spectra were shifted according to the experimental value to account for the systematic error introduced by the TDDFT method.

2.3 Multiconfigurational Self-Consistent Field Method

2.3.1 Background

The multiconfigurational self-consistent field method considers multiple electronic configurations of the same spin at the same time with a wavefunction expressed as a linear combination of multiple Slater determinants.²⁵

$$|\psi_{MCSCF}\rangle = \sum_i C_i |\Phi_i\rangle \quad (4)$$

Each Slater determinant is a linear combination of molecular orbitals with different occupation numbers.

$$|\Phi_i\rangle = \sum_k c_k |\phi_k\rangle \quad (5)$$

During the optimization, the MCSCF method optimizes both the expansion coefficients C_i for the configurations and the shared coefficients c_k for the molecular orbitals. The time complexity

can be extremely high for all possible configurations, so a reference is required to narrow the range of configurations of interest.

The generalized active space self-consistent field method (GASSCF) can serve as an effective reference for MCSCF.^{29,30} As shown in Figure 1, the orbitals are divided into five categories and placed into their corresponding subspaces, including the frozen doubly occupied orbitals, restricted doubly occupied orbitals, generalized active space (GAS), restricted unoccupied orbitals, and frozen unoccupied orbitals. With some orbitals that are less likely to participate in electronic interactions restricted as doubly occupied, the required computational resource can be dropped to an affordable level.

Besides the above formalism, there are advanced techniques that are used to enhance the accuracy of the computational results and optimize the calculation. Since the calculation focuses on the core electrons, which are close to the nucleus and move at a high speed, the scalar relativistic treatment is introduced *via* the exact-two-component approach (X2C).³¹ This method also requires the use of special basis sets that allow the calculation accounting for the relativist effect, such as the Douglas-Kroll (DK) basis sets. The driven similarity renormalization group method (DSRG) is another technique, providing high-accuracy results and great performance by eliminating the high-energy components in the Hamiltonian to reduce the computational complexity of the electronic configurations using a set of polynomial equations.³² The DSRG with multireference perturbation theory (DSRG-MRPT) is found to provide accurate results.³³

2.3.2 Computation Setup

The GASSCF formalism implemented in the Forte package was utilized as a reference with the cc-pCVQZ-DK basis set.^{22,23} The spin-adapted third-order DSRG-MRPT method (SA-DSRG-MRPT3) and the X2C approach were employed.

Active Space Selection. The selection of the generalized active space is essential for the computation as it needs to balance the tradeoff between accuracy and cost. A large active space may require unaffordable computational resources, while a small active space may not capture the electron correlations necessary for describing the system. As proposed in a similar procedure, it is necessary to include both the highest occupied molecular orbitals (HOMO) and a small number of virtual unoccupied orbitals in active space.³⁴ As the example GAS selection for CF₄ in Figure 1, six to seven frontier orbitals were included in the GAS to balance the performance and accuracy.

Root Number. The approximate number of root states to be found was determined assuming the single-electron excitation framework. Namely, the core electron is assumed to be excited from one molecular orbital in GAS1 to the unoccupied orbitals in GAS2. The symmetry for the final electronic state was calculated based on the product table for the irreducible representation. It should be noted, however, that this method still uses the multi-determinantal wave function to represent each core-excited electronic state.

Ground State Energy Shift. The energy difference between any two electronic states was calculated. The excitation energy of interest was computed as the energy difference between the ground state and the core-excited state. Due to the use of the MCSCF method, both the expansion coefficients for the configurations and the shared molecular orbital coefficients were

optimized solely based on the core-excited states. This results in potentially inaccurate energy of the ground state, leading to a systematic error in the excitation energies. Therefore, an independent calculation of the ground state energy was performed with all the molecular orbitals restricted to be doubly occupied except those in GAS2 to evaluate and correct the error introduced by the optimization for the core-excited states.

3. Results

3.1 Geometry and Energetics

As shown in Table 1, the energy of the molecules of interest (**1-5**) decreases by around 100 Hartree for each additional fluorine atom. In addition, the C-F bond length decreases in the molecules with more fluorine atoms. As shown in Figure 2, the molecular orbital diagram for each molecule of interest was calculated and visualized based on the orbital energy. The molecular orbitals show more character of degeneracy in the molecules with higher symmetry. The HOMO-LUMO energy gap first decreases and then increases as more fluorine atoms are introduced to the molecule. The carbon *1s*-like molecular orbital was found to be non-degenerate, whose energy decreases from -11.2 to -11.6 Hartree with the substitution of fluorine atoms. The fluorine *1s*-like orbitals demonstrated a gradual decrease in their orbital energy with more fluorine atoms introduced.

3.2 XANES Spectral Features

As shown in Table 2 and Table 3, the carbon and fluorine K-edge X-ray absorption peaks and intensities of each molecule were calculated using the TDDFT and the DSRG-MRPT3 method. The corresponding Lorentzian-transformed spectra were plotted as shown in Figure 3 and Figure 4. A shift of +10.9347 eV was applied to the carbon K-edge spectra based on the

difference between the experimental and the calculated value using the TDDFT method. The spectra calculated with the TDDFT method showed a higher number of peaks due to the large number of acceptor molecular orbitals (all unoccupied orbitals) compared with the spectra simulated using the DSRG-MRPT3 method focusing only on a small subspace of the unoccupied orbitals. In addition, the peak intensities for the spectra computed using the two methods were found to differ noticeably.

The carbon K-edge spectra showed a gradual increase in the transition energy with a range of 11.32 eV and 11.36 eV for the TDDFT method and DSRG-MRPT3 method with the increasing number of fluorine atoms, consistent with the experimental shift of 10.6 eV. With a decreased symmetry of the molecule, more spectral peaks were present compared with the ones with high symmetry. Similarly, the fluorine K-edge spectra demonstrated an increase in the excitation energy by 3.59 eV and 5.33 eV, slightly larger than the experimental shift in the binding energy of around 2.6 eV. For the methane molecule, the first spectral peak of its carbon K-edge XANES was calculated to have a zero intensity but was observed in the experimental spectrum.

3.3 Excitation Contribution

The dominant contribution from each excitation in each core-excited electronic state was calculated and summarized in Table 4 and Table 5. The carbon and fluorine K-edge core excitations identified by the TDDFT method were all found to contain one dominant contribution with a weight of more than 70%. Using the TDDFT method, the carbon K-edge core excitation for CH_3F and CF_4 showed some degree of multireference character, with peaks involving the mixing of two molecular orbitals. As for the fluorine K-edge spectra, the multireference

character increases along with the number of fluorine atoms, showing similarly weighted excitations. The results calculated by the DSRG-MRPT3 method were found to agree with the TDDFT method for the carbon K-edge spectra in terms of multireference character, while relatively similar multireference characters were manifested in CH_2F_2 , CHF_3 , and CF_4 in the fluorine K-edge XANES. The major difference in the attribution using the two methods was found to be the inclusion of electronic configurations with more than one excited electron, especially for the fluorine K-edge excitations. Multiple doubly excited electronic configurations were present in the attribution of excited states for the fluorine K-edge XANES with a weight from 2-7 %.

4. Discussion

As shown in Figure 3 and Figure 4, the carbon and fluorine K-edge XANES both have a gradual increase in the absorption peaks as the number of fluorine atoms increases. This may be due to the electron-withdrawing effect of the electronegative atoms that increases the orbital energy of the unoccupied orbitals, resulting in a blue shift of the transition peaks. This effect can suggest that the XANES can be used to detect the change in the electronegativity of the substituent groups of an atom. Since the shift for carbon is larger for fluorine atoms in this experiment, it is possible to employ this feature and probe the distance of the reaction to the moiety of interest.

The intensities calculated by the DSRG-MRPT3 method and the TDDFT method have a noticeable difference. The results calculated by the DSRG-MRPT3 method are consistent with the experimental spectra for the carbon K-edge XANES.¹⁵ Since the intensity for a peak is dependent on the overlap between the two orbitals involved in the transition, it can be

determined that the peaks with high intensities can be dominantly attributed to the transition between two molecular orbitals with the same angular quantum number. Therefore, for the excitation from the $1s$ -like orbitals, peaks with a higher intensity can demonstrate a high p -character of the dominant molecular orbital. In addition, there are peaks with zero intensity based on the results of the calculation that are present in the experimental spectra. For instance, the transition from $1s$ to $3s$ orbitals was predicted to have no intensity using the two methods. This discrepancy can be attributed to the vibronic coupling, which allows the weak $1s \rightarrow 3s$ transition.

As shown in the previous discussion, TDDFT as a single-reference method cannot fully capture the non-dynamic (static) electron correlation. To improve the accuracy of the calculations, the parameters of the calculations can be further tuned with more trials, including the functional selection. The performance of the TDDFT method can be influenced significantly by the selection of the functional. The functional should also be selected based on the specific system and reflect the time dependence, which can be selected to reflect the time dependence and thus decrease the systematic shift and accuracy. As for the DSRG-MRPT3 method, the active space involved in the GASSCF calculation can be extended to around a dozen orbitals to get a more complete K-edge XANES considering the contribution from more orbitals.

5. Code Availability

The code used in this project for geometry optimization and spectrum generation with TDDFT, and DSRG-MRPT2 is available in the GitHub repository [here](#).

6. References

- (1) Yano, J.; Yachandra, V. K. X-Ray Absorption Spectroscopy. *Photosynth Res* **2009**, *102* (2), 241.
- (2) Henderson, G. S.; de Groot, F. M. F.; Moulton, B. J. A. X-Ray Absorption Near-Edge Structure (XANES) Spectroscopy. *Reviews in Mineralogy and Geochemistry* **2014**, *78* (1), 75–138.
- (3) Schwarz, H. Chemistry with Methane: Concepts Rather than Recipes. *Angewandte Chemie International Edition* **2011**, *50* (43), 10096–10115.
- (4) Nagase, S.; Tanaka, K.; Baba, H. Direct Preparation of Partially Fluorinated Methane. *BCSJ* **1965**, *38* (5), 834–838.
- (5) MUIR, M. A Systematic Density Functional Study of Fluorination in Methane, Ethane and Ethylene. *Molecular Physics* **1996**, *89* (1), 211–237. <https://doi.org/10.1080/002689796174092>.
- (6) Castejon, H. J.; Wiberg, K. B. Effect of Fluorine Substitution on the Carbon Acidity of Methane, Methyl Isocyanide, Acetonitrile, Acetaldehyde, and Nitromethane. *J. Org. Chem.* **1998**, *63* (12), 3937–3942.
- (7) Koh, J. H.; Zakaria, Z. Hydrocarbons as Refrigerants? A Review. *ASEAN Journal on Science and Technology for Development* **2017**, *34* (1), 35–50. <https://doi.org/10.29037/ajstd.73>.
- (8) Solomon, K. R.; Velders, G. J. M.; Wilson, S. R.; Madronich, S.; Longstreth, J.; Aucamp, P. J.; Bornman, J. F. Sources, Fates, Toxicity, and Risks of Trifluoroacetic Acid and Its Salts: Relevance to Substances Regulated under the Montreal and Kyoto Protocols. *Journal of Toxicology and Environmental Health, Part B* **2016**, *19* (7), 289–304.
- (9) Velders, G. J. M.; Fahey, D. W.; Daniel, J. S.; McFarland, M.; Andersen, S. O. The Large Contribution of Projected HFC Emissions to Future Climate Forcing. *Proceedings of the National Academy of Sciences* **2009**, *106* (27), 10949–10954.
- (10) Li, Y.-X.; Zhang, Z.-Y.; An, M.-D.; Gao, D.; Yi, L.-Y.; Hu, J.-X. The Estimated Schedule and Mitigation Potential for Hydrofluorocarbons Phase-down in China. *Advances in Climate Change Research* **2019**, *10* (3), 174–180.
- (11) Chun, H.-U. Fine Structure of the X-Ray K-Absorption Edge of Carbon in Methane. *Physics Letters A* **1969**, *30* (8), 445–446.
- (12) LaVilla, R. E. Carbon and Fluorine X-ray Emission and Fluorine K Absorption Spectra of the Fluoromethane Molecules, CH₄–nFn (0 ≤ n ≤ 4). II. *J. Chem. Phys.* **1973**, *58* (9), 3841–3848.
- (13) Kincaid, B. M.; Eisenberger, P.; Hodgson, K. O.; Doniach, S. X-Ray Absorption Spectroscopy Using Synchrotron Radiation for Structural Investigation of Organometallic

Molecules of Biological Interest. *Proceedings of the National Academy of Sciences* **1975**, *72* (6), 2340–2342.

(14) Eberhardt, W.; Haelbich, R.-P.; Iwan, M.; Koch, E. E.; Kunz, C. Fine Structure at the Carbon 1s K Edge in Vapours of Simple Hydrocarbons. *Chemical Physics Letters* **1976**, *40* (2), 180–184.

(15) Brown, F. C.; Bachrach, R. Z.; Bianconi, A. Fine Structure above the Carbon K-Edge in Methane and in the Fluoromethanes. *Chemical Physics Letters* **1978**, *54* (3), 425–429.

(16) Dreuw, A.; Head-Gordon, M. Single-Reference Ab Initio Methods for the Calculation of Excited States of Large Molecules. *Chem. Rev.* **2005**, *105* (11), 4009–4037.

(17) Lischka, H.; Nachtigallová, D.; Aquino, A. J. A.; Szalay, P. G.; Plasser, F.; Machado, F. B. C.; Barbatti, M. Multireference Approaches for Excited States of Molecules. *Chem. Rev.* **2018**, *118* (15), 7293–7361.

(18) Smith, D. G. A.; Burns, L. A.; Simmonett, A. C.; Parrish, R. M.; Schieber, M. C.; Galvelis, R.; Kraus, P.; Kruse, H.; Di Remigio, R.; Alenaizan, A.; James, A. M.; Lehtola, S.; Misiewicz, J. P.; Scheurer, M.; Shaw, R. A.; Schriber, J. B.; Xie, Y.; Glick, Z. L.; Sirianni, D. A.; O'Brien, J. S.; Waldrop, J. M.; Kumar, A.; Hohenstein, E. G.; Pritchard, B. P.; Brooks, B. R.; Schaefer, H. F.; Sokolov, A. Yu.; Patkowski, K.; DePrince, A. E.; Bozkaya, U.; King, R. A.; Evangelista, F. A.; Turney, J. M.; Crawford, T. D.; Sherrill, C. D. PSI4 1.4: Open-Source Software for High-Throughput Quantum Chemistry. *J. Chem. Phys.* **2020**, *152* (18), 184108.

(19) Neese, F. The ORCA Program System. *WIREs Computational Molecular Science* **2012**, *2* (1), 73–78.

(20) Forte. <https://github.com/evangelistalab/forte> (accessed 2023-03-26).

(21) Hanwell, M. D.; Curtis, D. E.; Lonie, D. C.; Vandermeersch, T.; Zurek, E.; Hutchison, G. R. Avogadro: An Advanced Semantic Chemical Editor, Visualization, and Analysis Platform. *J. Cheminformatics.* **2012**, *4* (1), 17.

(22) Dunning, T. H. Gaussian Basis Sets for Use in Correlated Molecular Calculations. I. The Atoms Boron through Neon and Hydrogen. *J. Chem. Phys.* **1989**, *90* (2), 1007–1023.

(23) Woon, D. E.; Dunning, T. H. Gaussian Basis Sets for Use in Correlated Molecular Calculations. V. Core-valence Basis Sets for Boron through Neon. *J. Chem. Phys.* **1995**, *103* (11), 4572–4585.

(24) Casida, M. E. Time-Dependent Density-Functional Theory for Molecules and Molecular Solids. *Journal of Molecular Structure: THEOCHEM* **2009**, *914* (1), 3–18.

(25) Schuth, N. Combination of Advanced X-Ray Spectroscopy and Quantum Chemistry to Determine Electronic Structures of Metal-Organic Cofactors in Proteins. **2018**.

- (26) Becke, A. D. Density-functional Thermochemistry. III. The Role of Exact Exchange. *J. Chem. Phys.* **1993**, *98* (7), 5648–5652.
- (27) Lee, C.; Yang, W.; Parr, R. G. Development of the Colle-Salvetti Correlation-Energy Formula into a Functional of the Electron Density. *Phys. Rev. B* **1988**, *37* (2), 785–789.
- (28) de Jong, W. A.; Harrison, R. J.; Dixon, D. A. Parallel Douglas–Kroll Energy and Gradients in NWChem: Estimating Scalar Relativistic Effects Using Douglas–Kroll Contracted Basis Sets. *J. Chem. Phys.* **2001**, *114* (1), 48–53.
- (29) Ma, D.; Li Manni, G.; Gagliardi, L. The Generalized Active Space Concept in Multiconfigurational Self-Consistent Field Methods. *J. Chem. Phys.* **2011**, *135* (4), 044128.
- (30) Vogiatzis, K. D.; Li Manni, G.; Stoneburner, S. J.; Ma, D.; Gagliardi, L. Systematic Expansion of Active Spaces beyond the CASSCF Limit: A GASSCF/SplitGAS Benchmark Study. *J. Chem. Theory Comput.* **2015**, *11* (7), 3010–3021.
- (31) Cheng, L.; Gauss, J. Analytic Energy Gradients for the Spin-Free Exact Two-Component Theory Using an Exact Block Diagonalization for the One-Electron Dirac Hamiltonian. *J. Chem. Phys.* **2011**, *135* (8), 084114.
- (32) Evangelista, F. A. A Driven Similarity Renormalization Group Approach to Quantum Many-Body Problems. *J. Chem. Phys.* **2014**, *141* (5), 054109.
- (33) Li, C.; Evangelista, F. A. Driven Similarity Renormalization Group: Third-Order Multireference Perturbation Theory. *J. Chem. Phys.* **2017**, *146* (12), 124132.
- (34) Montorsi, F.; Segatta, F.; Nenov, A.; Mukamel, S.; Garavelli, M. Soft X-Ray Spectroscopy Simulations with Multiconfigurational Wave Function Theory: Spectrum Completeness, Sub-EV Accuracy, and Quantitative Reproduction of Line Shapes. *Journal of chemical theory and computation* **2022**, *18* (2), 1003–1016.

7. Tables/Figures/Schemes

Table 1. The energy and geometry of methane and its fluorinated derivatives at the CCSD(T)/cc-pCVDZ level of theory with the ZPVE correction.

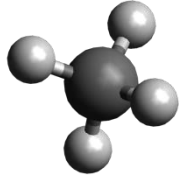
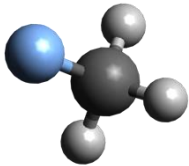
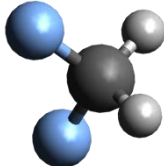
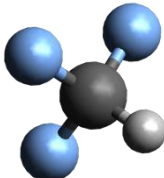
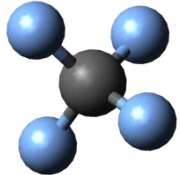
Compound	Structure	C – F bond length (Å)	C – H bond length (Å)	Energy (Hartree)	Energy with ZPVE (Hartree)
1		-	1.102	-40.4268198	-40.38194880
2		1.384	1.105	-139.488685	-139.44929351
3		1.360	1.104	-238.573555	-238.54043632
4		1.340	1.101	-337.671862	-337.64609038
5		1.326	-	-436.768101	-

Table 2. The peaks and corresponding intensities of carbon K-edge core excitations for methane and its fluorinated derivatives calculated using the TDDFT at the B3LYP/cc-pVQZ-DK level of theory and DSRG-MRPT3 with a GASSCF reference with the cc-pCVQZ-DK basis set and spin-free exact-two-component one-electron treatment.

Molecule	Calculated				Experimental ¹⁵	
	TDDFT		DSRG-MRPT3			
	Peak (eV)	Intensity	Peak (eV)	Intensity		
CH ₄	1	275.97 (0.00)	0	287.82 (0.00)	0.000	287.0 (0.0)
	2	277.57 (1.60)	2189	289.71 (1.89)	0.168	288.1 (1.1)
CH ₃ F	1	278.12 (0.00)	649	290.36 (0.00)	0.031	289.1 (0.0)
	2	278.75 (0.63)	220	290.89 (0.53)	0.012	290.5 (1.4)
	3	279.61 (1.49)	1769	291.84 (1.48)	0.055	291.6 (2.5)
CH ₂ F ₂	1	280.60 (0.00)	666	293.14 (0.00)	0.032	291.9 (0.0)
	2	281.09 (0.49)	1170	293.28 (0.14)	0.059	292.9 (1.0)
	3	281.66 (1.06)	1005	294.19 (1.05)	0.050	294.0 (2.1)
	4	282.10 (1.50)	283	294.83 (1.69)	0.027	294.5 (2.6)
CHF ₃	1	283.21 (0.00)	820	295.93 (0.00)	0.031	294.8 (0.0)
	2	284.13 (0.92)	3077	296.39 (0.46)	0.075	295.3 (0.5)
	3	285.78 (2.57)	160	296.64 (0.71)	0.098	297.2 (2.4)
	4	287.81 (4.60)	2395	298.97 (3.04)	0.032	298.0 (3.2)
CF ₄	1	287.29 (0.00)	0	299.18 (0.00)	0.133	297.6 (0.0)
	2	287.51 (0.22)	7607	299.26 (0.08)	0.106	298.0 (0.4)
	3	289.95 (2.66)	3499	299.35 (0.17)	0.098	298.5 (0.9)
	4	290.86 (3.57)	0	300.97 (1.79)	0.001	298.9 (1.3)

Table 3. The peaks and corresponding intensities of fluorine K-edge core excitations for methane and its fluorinated derivatives calculated using the TDDFT at the B3LYP/cc-pVQZ-DK level of theory and DSRG-MRPT3 with a GASSCF reference with the cc-pCVQZ-DK basis set and spin-free exact-two-component one-electron treatment.

Molecule	Calculated				Binding Energy ¹² Peak (eV)	
	TDDFT		DSRG-MRPT3			
	Peak (eV)	Intensity	Peak (eV)	Intensity		
CH ₃ F	1	670.70 (0.00)	11	689.35 (0.00)	0.011	
	2	670.94 (0.24)	561	690.45 (1.10)	0.004	
	3	672.38 (1.68)	51	692.13 (2.78)	0.001	692.4
CH ₂ F ₂	1	671.59 (0.00)	22	692.68 (0.00)	0.116	
	2	672.19 (0.60)	450	692.94 (0.26)	0.001	
	3	672.82 (1.23)	18	694.40 (1.72)	0.000	693.2
	4	672.83 (1.24)	286	696.53 (3.85)	0.012	
CHF ₃	1	672.51 (0.00)	37	694.96 (0.00)	0.093	694.1
	2	673.54 (1.03)	466	695.87 (0.91)	0.001	
	3	673.73 (1.22)	241	695.89 (0.93)	0.045	
	4	674.67 (2.16)	188	696.53 (1.57)	0.000	
	5	676.31 (3.80)	747	698.03 (3.07)	0.008	
	6	677.37 (4.86)	1	698.45 (3.49)	0.005	
	7	677.39 (4.88)	20	699.93 (4.07)	0.010	
	8	678.87 (6.36)	171	701.49 (6.53)	0.003	
CF ₄	1	674.29 (0.00)	361	694.68 (0.00)	0.065	695.0
	2	675.51 (1.22)	445	697.18 (2.50)	0.012	
	3	675.52 (1.23)	579	697.58 (2.90)	0.032	
	4	676.63 (2.34)	493	698.90 (4.22)	0.010	

Table 4. The significant ($w > 0.01$) contributions of individual excitations in the simulated carbon K-edge X-ray absorption spectra of $\text{CH}_n\text{F}_{4-n}$ using the TDDFT and the DSRG-MRPT3 method. The occupied orbitals are labeled -1, -2, ... as energy decreases and the virtual orbitals labeled 1, 2, ... as energy increases, which are represented by the number in the bracket. The donor energy level is assumed to be the level containing the GAS1 orbitals unless otherwise stated.

Molecule		Method	
		TDDFT	DSRG-MRPT3
CH ₄	1	1.00 (1)*	0.97 (1)
	2	0.98 {2} + 0.02 {5}	0.97 {2}
CH ₃ F	1	0.73 (1) + 0.25 [2]	0.63 [2] + 0.37 (3)
	2	0.26 (1) + 0.73 [2]	0.37 [2] + 0.63 (3)
	3	0.99 (3)	1.00 (1) 1.00 [2]
CH ₂ F ₂	1	0.94 (1) + 0.05 (4)	0.99 (1)
	2	0.96 (3) + 0.04(7)	0.99 (3)
	3	0.99 (2)	0.99 (2)
	4	0.05 (1) + 0.92 (4) + 0.02 (6)	0.99 (4)
CHF ₃	1	0.98 (1)	0.97 (1) + 0.02 (3)
	2	0.93 (1) + 0.07 [5]	0.83 [2] + 0.15 (3)
	3	0.97 (3) + 0.02 (4)	0.99 [2]
	4	0.03 (3) + 0.93 (4) + 0.02 (7)	0.15 [2] + 0.82 (3)
CF ₄	1	1.00 (1)	0.98 {2}
	2	0.79 {2} + 0.21 {3}	0.57 (1) + 0.41 {2}
	3	0.21 {2} + 0.79 {3}	0.99 {2}
	4	1.00 (4)	0.39 (1) + 0.58 {2}

*The energy level contains () no degenerate orbitals; [] doubly degenerate orbitals; and { } triply degenerate orbitals.

Table 5. The significant ($w > 0.01$) contributions of individual excitations in the simulated fluorine K-edge X-ray absorption spectra of $\text{CH}_n\text{F}_{4-n}$ using the TDDFT and the DSRG-MRPT3 method. The occupied orbitals are labeled -1, -2, ... as energy decreases and the virtual orbitals labeled 1, 2, ... as energy increases, which are represented by the number in the bracket. The donor energy level is assumed to be the level containing the GAS1 orbitals and omitted unless otherwise stated.

Molecule	Method		
	TDDFT	DSRG-MRPT3	
CH3F	1	0.91 (1) + 0.09 [2]*	0.88 (1) + 0.12 [2]
	2	0.09(1) + 0.89[2] + 0.02(5)	0.12 (1) + 0.87 [2]
	3	1.00 [2]	1.00 [2] 1.00 (3)
CH2F2	1	0.99(1)	0.56(3) + 0.33(4) + 0.02 [-12], (-3)→ (3), (4)
	2	0.88(2) + 0.09(3)	0.86 (1) + 0.07 [-12], (-3)→ (1), (4) + 0.02 [-12], (-2)→ (1), (3)
	3	1.00(2)	0.87 (2) + 0.07 [-12], (-3)→ (2), (4) + 0.02 [-12], (-2) → (2), (3)
	4	0.10(3) + 0.87(4)	0.32 (3) + 0.53 (4) + 0.04 [-12], (-3) → (4) + 0.03 [-12], (-2) → (3), (4)
CHF3	1	0.99(1)	0.83 [2] + 0.08(3)
	2	0.89[2] + 0.06(3) + 0.02(4) + 0.03[5]	0.87(1) + 0.06 {-11}, (-2) → (1), [2]
	3	0.99[2]	0.03 (1) + 0.25[2] + 0.65(3)
	4	0.07[2] + 0.90(3) + 0.02(4)	0.87(1) + 0.03(3) + 0.04 {-11}, (-2) → (1), [2]
	5	0.03[2] + 0.03(3) + 0.52(4) + 0.39[5] + 0.03(6)	0.74[2] + 0.15(3) + 0.03 {-11}, (-2) → [2]
	6	0.99[5]	0.91[2] + 0.02 {-11}, (-2) → [2] + 0.02 {-11}, (-2) → [2], (3)
	7	0.43(4) + 0.56[5]	0.24[2] + 0.64 (3) + 0.03 {-11}, (-2) → [2], (3)
	8	0.95 (6)	0.64 [2] + 0.24(3) + 0.03 {-11}, (-2) → [2] + 0.02 {-11}, (-2) → [2], (3)
CF4	1	0.83(1) + 0.12{2} + 0.03(4)	0.42 (1) + 0.49{2}
	2	0.17(1) + 0.61{2} + 0.17{3} + 0.05(4)	0.47 (1) + 0.41{2} + 0.02 [[-9]], {-1} → (1), {2}
	3	0.96{2} + 0.04{3}	0.90 {2} + 0.07 [[-9]], {-1} → {2}
	4	0.26 {2} + 0.46{3} + 0.27(4)	0.88 {2} + 0.04 [[-9]], {-1} → {2}

*The energy level contains () no degenerate orbitals; [] doubly degenerate orbitals; { } triply degenerate orbitals; and [] quadruply degenerate orbitals.

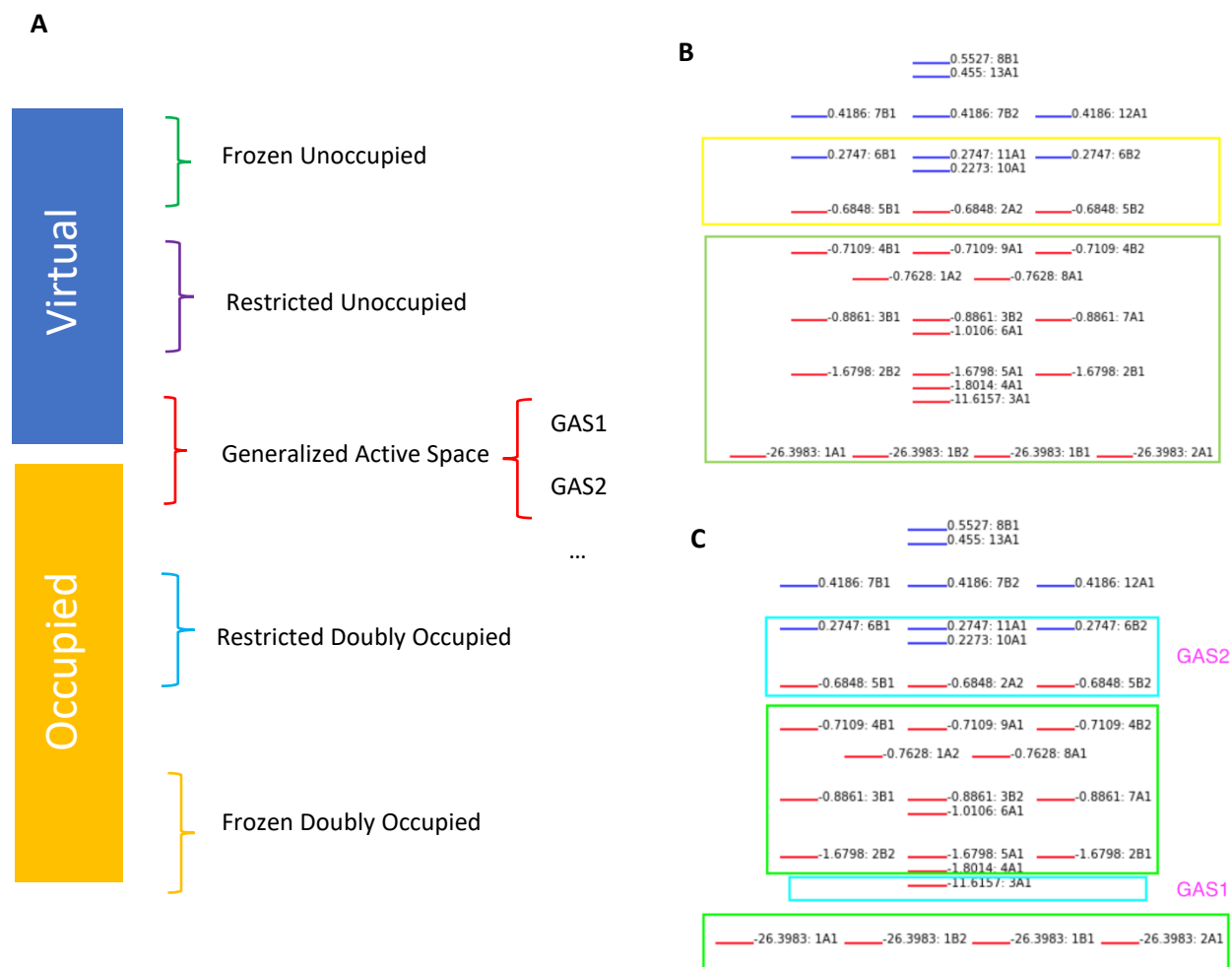


Figure 1. (A) The active space selection scheme for GASSCF method. (B) The ground-state calculation for tetrafluoromethane with restricted doubly occupied orbitals (green) and active space (yellow). (C) The core-excited state calculation for tetrafluoromethane with restricted doubly occupied orbitals (green) and active space (blue), including GAS1 and GAS2.

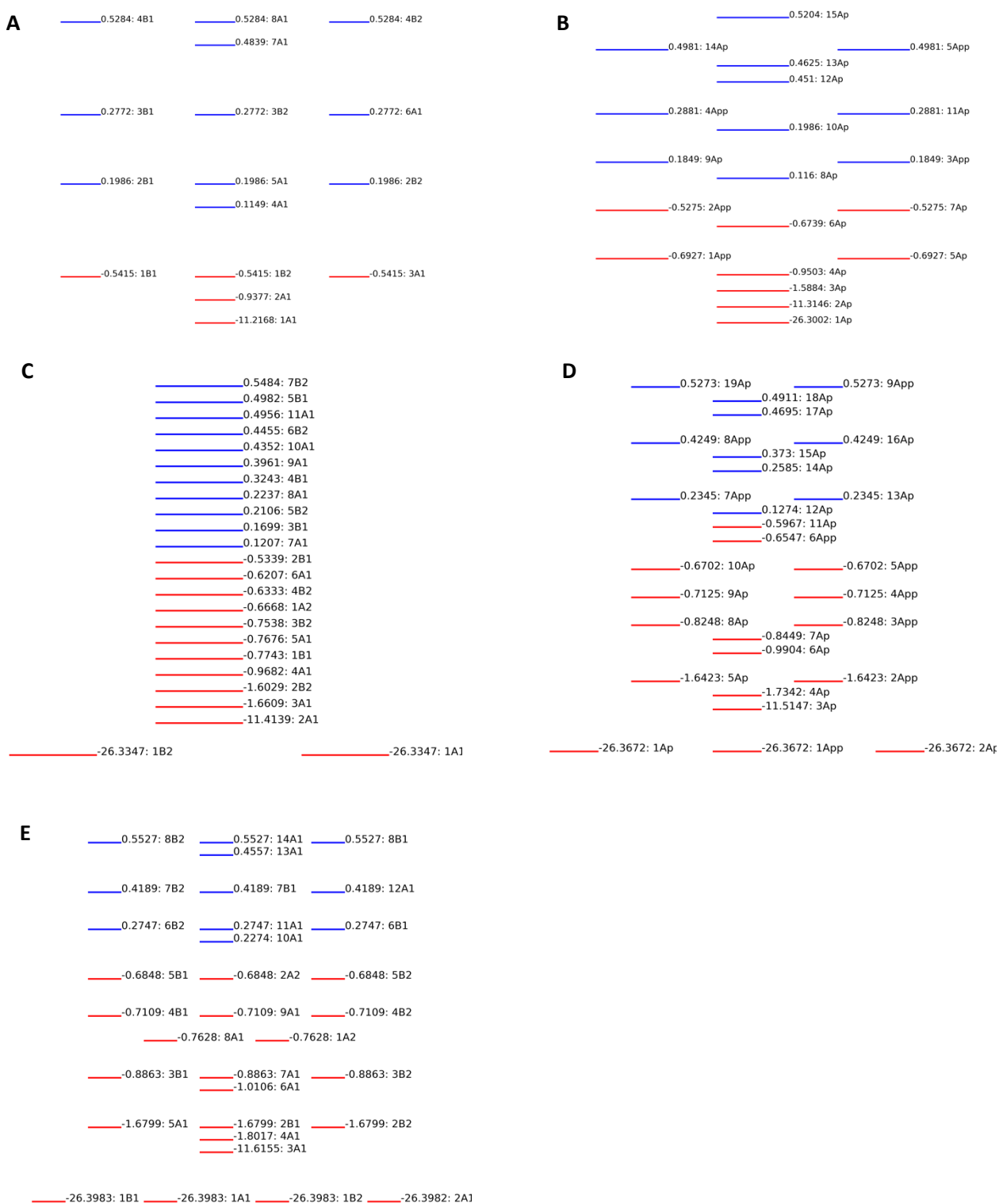


Figure 2. The orbital energy diagram of (A) CH₄, (B) CH₃F, (C) CH₂F₂, (D) CHF₃, and (E) CF₄ computed using the self-consistent Hartree-Fock method with the cc-pCVQZ-DK basis set. The doubly occupied molecular orbitals are colored red and the unoccupied blue. The orbital energy and irreducible representation are labeled along each orbital.

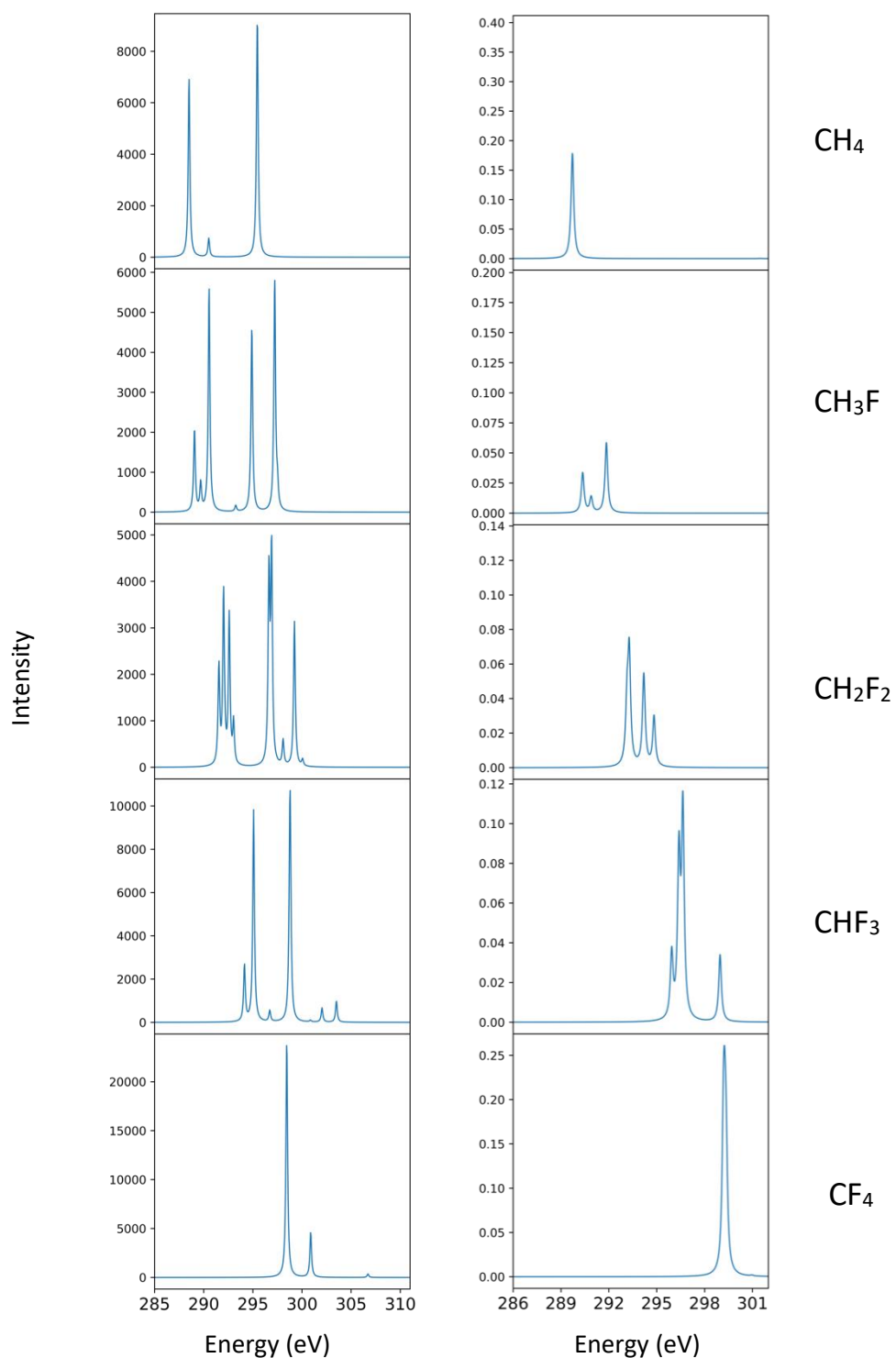


Figure 3. The carbon K-edge X-ray absorption near edge spectra (XANES) of fluorinated derivatives of methane calculated using TDDFT at the B3LYP/cc-pVQZ-DK level of theory (left) and DSRG-MRPT3 with a GASSCF reference with the cc-pCVQZ-DK basis set and spin-free exact-two-component one-electron treatment (right).

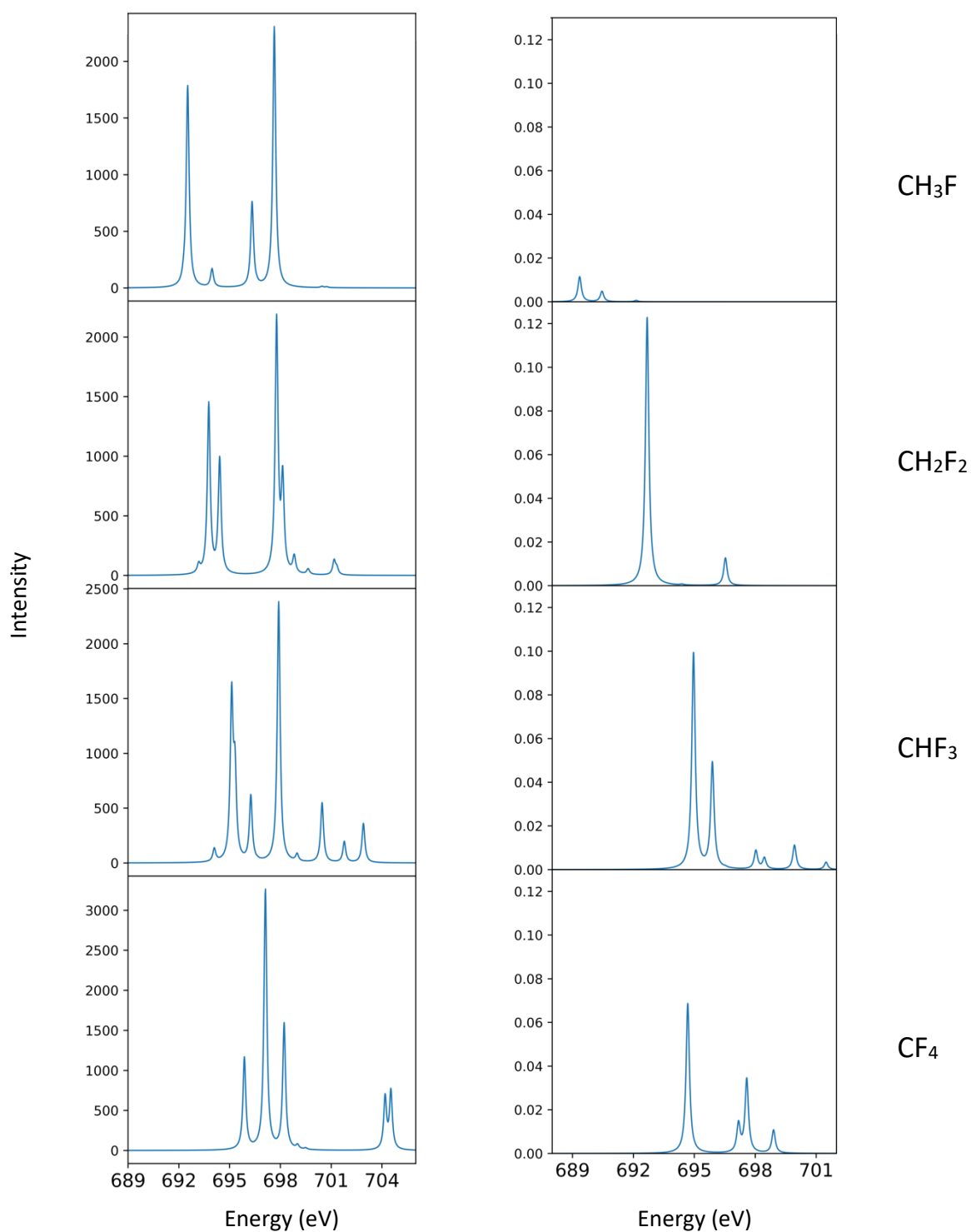


Figure 4. The fluorine K-edge X-ray absorption near edge spectra (XANES) of fluorinated derivatives of methane calculated using TDDFT at the B3LYP/cc-pVQZ-DK level of theory (left) and DSRG-MRPT3 with a GASSCF reference with the cc-pCVQZ-DK basis set and spin-free exact-two-component one-electron treatment (right).